ISSN 0016-7932, Geomagnetism and Aeronomy, 2013, Vol. 53, No. 1, pp. 85–95. © Pleiades Publishing, Ltd., 2013.
Original Russian Text © M. Förster, Y.I. Feldstein, L.I. Gromova, L.A. Dremukhina, A.E. Levitin, S.E. Haaland, 2013, published in Geomagnetizm i Aeronomiya, 2013, Vol. 53, No. 1, pp. 91–101.

Some Aspects of Modelling the High-Latitude Ionospheric Convection from Cluster/Edi Data[1]

M. Förster[a], Y. I. Feldstein[b], L. I. Gromova[b], L. A. Dremukhina[b], A. E. Levitin[b], and S. E. Haaland[c]

[a] *Helmholtz–Zentrum Potsdam, GFZ German Research Centre for Geosciences, Potsdam, Germany*

[b] *Pushkov Institute of Terrestrial Magnetism, Ionosphere, and Radiowave Propagation (IZMIRAN), Troitsk, 142090 Russia*

[c] *Department of Physics and Technology, University of Bergen, Norway*

e-mail: gromova@izmiran.ru

Received July 25, 2011; in final form, July 07, 2012

Abstract—Measurements onboard Cluster satellites are briefly described, which form the base for determining the intensity and direction of the electric field in the magnetosphere. The aim of this paper is to describe (1) the methodology of calculating the potential distribution at the ionospheric level and the results of constructing spatiotemporal convection patterns for different orientations of the IMF vector in the GSM *YZ* plane; (2) derivation of basic convection patterns (BCPs), which allow to deduce the statistical ionospheric convection pattern at high latitudes for any IMF *Bz* and *By* values (statistical convection model) using different sets of independent data; (3) the consequences of enlarging the amount of data used for analysis; (4) the results of potential calculations with various orders of the spherical harmonics describing them; (5) determination of the cross-polar cap potential with different IMF sector widths (α from 45° down to 10°); (6) the results of our trials to determine the contribution of the IMF *Bx* component to the convection pattern.

DOI: 10.1134/S001679321301009X

1. INTRODUCTION

A group of four identical Cluster satellites has been performing plasma measurements in large ranges of the Earth's magnetosphere and beyond since February 2001. The Electron Drift Instrument (EDI) onboard Cluster measures the 2–D drift velocity of artificially injected electrons perpendicular to the local geomagnetic field. The EDI emits two low-intensity 1-keV electron beams and receives the returning beam after one or more gyrations in the surrounding magnetic field. Due to cycloidal motion, an electron beam can only be recorded when fired in a particular direction, which is unambiguously determined by the intensity and direction of the plasma drift. The measurement principle requires the continuous tracking of true changes for these firing directions. The drift vector is estimated by the triangulation of the two beams or from the difference between their time-of-flight values (Paschmann et al., 2001).

The observed minimum drift velocity amounts to ~1 km/s, which corresponds to ~0.1 mV/m for a magnetic field strength of ~100 nT in the magnetosphere. An important advantage of the EDI technique for measurements at high altitudes consists in its insensitivity to wake effects, which influences electric field measurements by means of plasma probes in low-density environments of the outer magnetosphere (Eriksson et al., 2006). The EDI performs electric field measurements with a time resolution of ≤10 Hz (depending on the beam return); for this study, we use 1-min average values only.

The satellites moved along an excentric near-polar orbit with an initial apogee and perigee of ~4 and ~19.6 R_E, respectively, and an orbital period of ~57 h. The orbital precession rate is such that all magnetic local times (MLT) of both polar caps (above an invariant latitudes $\Phi > \sim 74°$) are covered twice per year with observations. The spacecraft's velocity is about 3 to 4 km/s for typical overflights above the polar cap. The distance between individual data points after their mapping from the magnetospheric measurement point onto the ionosphere at an altitude of ~400 km amounts to about ~2 km in latitude and ~20 km in longitude. Due to precession constraints, the local time coverage of data points, mapped to magnetic latitudes $\Phi < 74°$, changes with the season. During summer months in the Northern Hemisphere (June–August), the daytime (afternoon) sector is covered, while during the northern winter months (December–February) it is the nighttime (early morning) sector. For the global coverage over all MLT, data of at least one full calendar year are needed.

The magnetic field vector are measured onboard Cluster by means of a three-component fluxgate magnetometer (FGM), which is mounted at 5-m radial booms. The measurement interval in various operative ranges spans over ±4000 nT with a typical precision of ±0.1 nT (Balogh et al., 2001). For the mapping of elec-

[1] The article was translated by the authors.

tric field measurements from the magnetosphere to the ionosphere we use the Tsyganenko-2001 external geomagnetic field model (http://geo.phys.spbu.ru/~tsyganenko/modeling.html). The input parameter in this model comprises not only actual values of the solar wind velocity, density, and components of the interplanetary magnetic field (IMF), but also their values in the preceding hour.

In Section 2 we will briefly explain the methodology of determining the spatiotemporal electric field pattern depending on the IMF orientation, as it was described in detail in the papers of Haaland et al. (2007) and Förster et al. (2007, 2008). These patterns are then presented in Section 3. Section 4 presents some estimates of approximate patterns, which were also used for the construction of a statistical ionospheric convection model that describes the dependencies on IMF *By* and *Bz* (Förster et al., 2009); in Section 5 we illustrate our trials to derive a convection part that might be controlled by the IMF *Bx* component during time intervals when the IMF is northward ($Bz > 0$). In Section 6 we finally summarize the main findings of this study.

2. METHODOLOGY TO DETERMINE THE IONOSPHERIC ELECTRIC FIELD PATTERN

Solar wind parameters and IMF vector data were obtained from the ACE satellite near the *L1* libration point upstream of the Earth and time shifted to represent the IMF conditions at the frontside magnetopause (at $X_{GSM} = 10\ R_E$) using the phase front propagation technique (Weimer et al., 2003; Haaland et al., 2006). It assumes the existence of "phase fronts," which can adopt any angle with respect to the solar wind velocity and parallel to which the adjacent IMF orientation is supposed to propagate toward the Earth.

Cluster/EDI measurements are obtained far from the Earth's ionosphere. To derive the regularities of the ionospheric convection pattern, mapping of the observations to the ionospheric level is presumed. Such a procedure usually presupposes the existence of equipotentiality along geomagnetic field lines in correspondence with a geomagnetic field model (Baker et al., 2004).

Assuming the spacecraft is at a certain X_1^m position in the magnetosphere, its mapping point at an altitude of 400 km in the ionosphere X_1^i is uniquely determined by the model. Then the potential difference between X_1^m and position X_1^i, which is located at distance d^m in magnetospheric drift vector direction V^m, amounts to $\Delta\Phi^m = E^m d^m = V^m B^m d^m$, where E^m is the electric field in the magnetosphere, which is constant over distance d^m, and B^m is the magnetic field strength. The precision of electric field measurements by the EDI in the magnetosphere is between 0.1 and 0.2 mV/m.

Distance d^m of an order of ~1000 km was assumed in the dependence on the magnetic field magnitude ratio in the B^m magnetosphere and B^i ionosphere, so that it results in $d^i \sim 50$ km. The mapping of X_1^m to ionospheric point X_1^i determines the d^i value, which is the projection of d^i onto the ionosphere in magnitude and orientation. The potential difference over d^i is equal to $\Delta\Phi^i = E^i d^i = ViB^i d^i$. Under the assumption of equipotentiality along geomagnetic field lines, we have $\Delta\Phi^m = \Delta\Phi^i$, so that the electric field at ionospheric height amounts to $E^i = E^m d^m / d^i E^i$.

The electric field at upper ionospheric heights can be obtained from EDI measurements under the assumption that the geomagnetic field lines are frozen into the plasma flow (Haaland et al., 2007). The t^m time interval to move a magnetic field line from point X_1^m over distance d^m to X_2^m amounts to $t^m = d^m / V^m$, where V^m is the drift velocity in the magnetosphere as measured by the EDI. The t^i convection time of the plasma flow over distance d^i between the X_1^i and X_2^i points in the ionosphere, which are the projections of X_1^i and X_2^i, results in $t^i = d^i / V^i$. Under the frozen-in assumption, we have $t^i = t^m$ and, therefore, $V^i = V^m (d^i / d^m)$. Throughout the paper, we use ionospheric convection velocities V^i obtained from EDI observations in the spacious magnetosphere under the assumption of a frozen-in plasma flow.

3. CONVECTION AT HIGH LATITUDES FOR DIFFERENT IMF ORIENTATIONS

The measured EDI electric field vectors, mapped onto the high-latitude ionosphere and binned into 784 grid points within 32° of the magnetic colatitude range, were sorted and averaged with respect to the IMF orientation in the GSM *ZY* plane into eight sectors of 45° in width each. The bins have a 2° width in latitude and are variable in magnetic local time (MLT) in such a manner that the bins' areas are approximately of equal sizes with $\sim 5 \times 10^4$ km^2. The electric field grid is therefore equidistant in magnetic latitude (MLAT) and inhomogeneous in longitude (MLT).

The global convection pattern is established in terms of the electric potential distribution, U_i, based on the E_i electric field data at ionospheric levels, related by the expression

$$\vec{E} = -\vec{v} \times \vec{B} = -\text{grad}\Phi. \quad (1)$$

The plasma drift vector grid pattern is thus fitted to smoothed potential distribution U_i by minimizing the χ^2 quantity given by

$$\chi^2 = \sum_{i=1}^{N} \left| \vec{E}_i + \text{grad}\,\Phi \right|^2. \quad (2)$$

For an analytic presentation of the potential in the high-latitude region, bounded toward the equator at 58° geomagnetic latitude, we used spherical harmonic analysis (Haines, 1985). They were applied for each sector individually as a function of geomagnetic colatitude θ and MLT (via azimuthal angle φ)

$$U(\theta,\varphi) = \sum_{l=0}^{L} A_{l0} P_l^0(\cos\theta) + \sum_{l=0}^{L}\sum_{m=0}^{l} (A_{lm}\cos m\varphi + B_{lm}\sin m\varphi) P_l^m(\cos\theta), \quad (3)$$

where P_l^m are the associated Legendre polynomials with degree l and order m of the harmonic polynomials and A_{lm} and B_{lm} are the real parts of the coefficients, uniquely determined from the $N \times K$ matrix. Here, N is the number of grid points and K is the number of coefficients, determined by the number of the spherical harmonics used $L = 8$ or 10 (in our case) so that $K = (L + 1)^2$.

The spatiotemporal distribution of the electric potential at high latitudes was obtained by accumulating data on convection intervals with a well-established IMF orientation (Haaland et al., 2007). Figure 1 shows such potential distributions for eight different orientations (sectors) of the IMF near the magnetopause for the interval between February 2001 and April 2009, and Table 1 lists the mean values of the IMF components for the data points used in each sector. The isolines of Fig. 1 are plotted in altitude-adjusted corrected geomagnetic (AACGM) coordinates with 3-kV spacing, where the outer border of the dials is at 60° magnetic latitude. The EDI measurements predominantly occurred during moderate IMF vector amplitudes with median values of ~4 to 5 nT. The sector width is 45° of the IMF angle orientation in the GSM *YZ* plane with eight distinct sectors (from Sector 0 to 7), which are also 45° apart from each other, shifted in a clockwise direction. For the southward IMF (Sector 4), the convection pattern consists of two cells, the foci of which are located at Φ ~ 73° magnetic latitude on the morning side and at Φ ~ 75° on the evening side with antisolar-directed (from the dayside to the nightside) convection across the polar cap. The separation line between the two cells is approximately oriented along the noon to the midnight meridian. The cross-polar cap potential difference between the cell pair foci amounts to $\Delta U = 54.5$ kV, which is the maximum value of all eight IMF orientations (sectors).

For an east–west orientation of the IMF (Sector 2 for $By > 0$ and Sector 6 for $By < 0$), a two-cell convection pattern is retained. In the polar cap, there takes place a deformation of plasma convection cells: the area of the evening (morning) side cell increases in Sectors 2/6 in the case of the Northern Hemisphere (mirror symmetric in the Southern Hemisphere). The zero-potential line is shifted simultaneously toward the morning (evening) side.

Table 1. Median values of IMF *Bx*, *By*, and *Bz* on the magnetospheric boundary in the eight sectors for the time interval February 2001–April 2009

IMF Sector	Direction	*Bx*, nT	*By*, nT	*Bz*, nT
0	B_z^+	0.02	0.05	3.79
1	B_z^+/B_y^+	−1.54	3.13	2.66
2	B_y^+	−2.57	4.48	0.01
3	B_z^-/B_y^+	−2.48	3.23	−2.87
4	B_z^-	−1.46	−0.02	-4.82
5	B_z^-/B_y^-	2.19	−3.87	−3.3
6	B_y^-	2.84	−5.02	0.00
7	B_z^+/B_y^-	1.90	−3.81	3.00

For a northward-directed IMF (Sector 0), in addition to the two main (nightside) cells with $\Delta U \sim 12.8$ kV, there appears a further pair of convection cells at high dayside latitudes with $\Delta U \sim 11.4$ kV and sunward-directed convection (from the nightside toward the dayside) between them. According to Fig. 1, the main cell potential drop decreases steadily when turning from Sector 4 to Sector 0. The potential difference between the two cell pairs of Sector 0 only differs by 1.4 kV.

4. ESTIMATION OF THE POTENTIAL ACCURACY AND CONVECTION MODEL

Table 2 lists potential differences ΔU for various data sets, which allows one to evaluate the variation in these cross-polar potential drops depending on the length of the data sample interval and the degree of spherical harmonics (8 vs. 10) according to Eq. (3). For this analysis, we used partial data given in public literature (Haaland et al., 2007, 2009; Förster et al., 2009).

For data sets of the full interval 2001–2009 with both degree 8 and 10 of spherical harmonics, we get practically no difference for all 8 sectors. The scatter of the ΔU values is confined to 0.3 kV for the main cells and 0.1 kV for minor dayside cells at high latitudes (Sector 0).

The ΔU summer values are taken from Table 2 in (Förster et al., 2009). In order to achieve global data coverage, values for both Northern (March to September) and Southern (September to March) hemispheres were used. The latter subset was projected onto the Northern Hemisphere data set with an inverted sign of the IMF *By* component. The differences

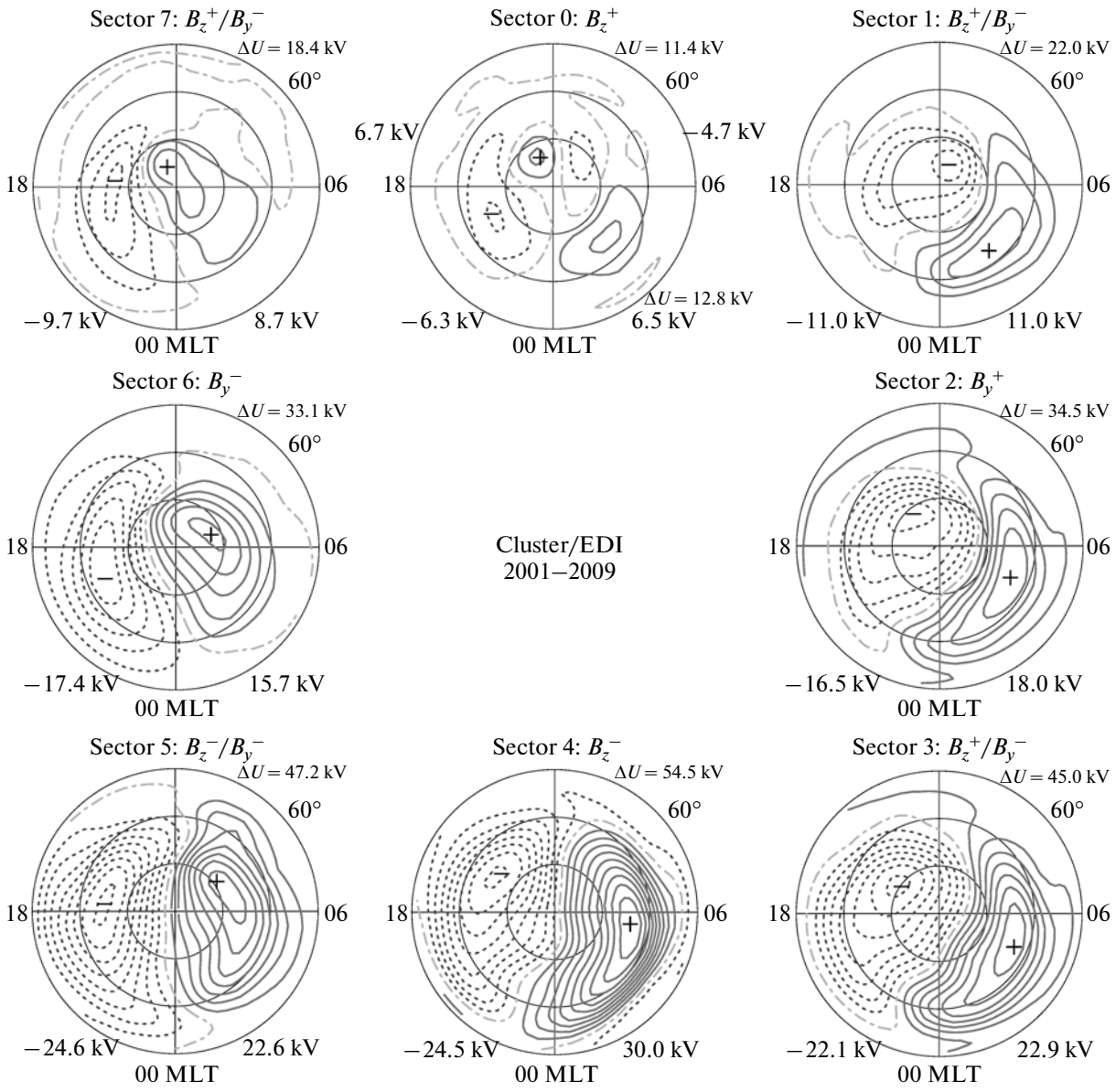

Fig. 1. Electric potential patterns obtained from Cluster C1–C3 EDI observations in the Northern Hemisphere as a function of magnetic latitude and magnetic local time for eight IMF clock-angle orientations (sectors). The positions of the maximum and minimum values are indicated by "+" and "–" sign, respectively, and their values are shown at the bottom of each panel. Total cross-polar cap potential difference ΔU is indicated at the upper right corner for each sector. For Sector 0 (IMF $Bz > 0$), the maximum and minimum values for high-latitude dayside cells are also shown. Positive and negative potential values are displayed with continuous and dashed lines, respectively, while their spacing is 3 kV.

between the potential drops between the full-year and summer sets are of an order of a few kilovolts with an average difference of ~4 kV, where higher values are observed for all sectors of the summer data set, except for Sector 5. The high-latitude dayside pair of Sector 0 only differs by $\Delta U = 0.4$ kV, the three northward-directed IMF sectors (7, 0, and 1) have an average difference of $\Delta U = 2.2$ kV, and the three southward-directed IMF sectors (3–5) scatter around ~6.0 kV.

The augmentation of the data volume from about 5 years (February 2001–March 2006) to about 8 years (February 2001–April 2009) is accompanied by a change in the cross-polar cap potential differences: it diminishes by 1.4 kV for high-latitude dayside cells and by 7.3 and 2.2 kV for the southward and northward IMF, respectively.

The statistical convection model offered by Förster et al. (2009) based on Cluster EDI measurements sug-

Table 2. Cross-polar cap potential ΔU (kilovolt) difference between high-latitude convection foci in the Northern Hemisphere for Cluster/EDI measurements

IMF Sector	ΔU, kV 2001–2006 (8 harmonics)[1]	ΔU, kV 2001–2009 (8 harmonics)[2]	ΔU, kV 2001–2009 (10 harmonics)[3]	ΔU, kV 2001–2008, summer (10 harmonics)[4]
0	12.8 (dayside)	11.4	11.4	11.0
	14.3 (hightside)	12.8	12.8	13.6
1	27.5	21.5	22.0	24.1
2	40.6	34.2	34.5	37.5
3	54.3	45.0	45.0	54.2
4	61.9	54.2	54.5	58.1
5	51.3	47.4	47.2	43.5
6	33.5	33.1	33.1	37.7
7	18.3	18.9	18.4	21.5

Note: [1] Haaland et al. (2007), [2] Haaland et al. (2009), [3] this study, and [4] Förster et al. (2009).

gests a linear relationship between the potential and the IMF *By* and *Bz* components:

$$U(\mathrm{MLAT},\mathrm{MLT},By,Bz) = U_0(\mathrm{MLAT},\ \mathrm{MLT}) + By\,U_y^{\pm} + Bz\,U_z^{\pm}, \quad (4)$$

where U_0 (in kilovolts) represents a constant term which is independent of the IMF, while the $U_y^{\pm}$ and $U_z^{\pm}$ terms (in kV/nT) describe the linear dependencies on the IMF *By* and *Bz* components, respectively, normalized to 1-nT variations, which can be different for different signs; coefficients $U_y^{\pm}$ and $U_z^{\pm}$ with upper indices "+" and "–" correspond to positive and negative IMF *By* or *Bz*, respectively. Plasma drift velocity measurements were mainly conducted for moderate *By* and *Bz* value (see Table 1), which justifies the use of linear relationships. Such a decomposition of the potential pattern dependencies has already been used previously in, e.g., (Feldstein and Levitin, 1986; Papitashvili and Rich, 2002; Kabin et al., 2003).

Figure 2 shows elements of the basic convection pattern (BCP): U_0 (upper left panel), $U_y^{\pm}$ (lower right panel for $By = \pm 1$ nT, drawn here for $By = 1$ nT), U_z^{+} (upper right panel with $Bz = +1$ nT) and, finally, U_z^{-} (lower left panel with $Bz = -1$ nT). The BCP elements are calculated from the summation of various potential patterns of the sectors in Fig. 1. The U_0 background potential for vanishing IMF *By* and *Bz* components (upper left panel) is derived as the sum of sectors 2 and 6 in Fig. 2, while the *By* dependence (lower right panel) is derived from their difference, normalized to $By = 1$ nT; U_z^{+} and U_z^{-} are determined as potential differences between sector 0 or sector 4, respectively, and the U_0 background potential, normalized to $Bz = +1$ nT or $Bz = -1$ nT.

The IMF-independent part of the potential, i.e., U_0, corresponds to a two-cell pattern with antisolar convection over the polar cap. An analoguous two-cell pattern displays the U_z^{-} potential. The U_z^{+} potential appears as a two-cell pattern with a concentration of isolines in the dayside high-latitude region, where convection is sunward directed. Finally, the $U_y^{\pm}$ potential corresponds to one-cell convection within the polar cap, the focus of which is close to its center. In the Northern Hemisphere, the plasma convection is clockwise for positive B_y^{+} and counterclockwise for negative B_y^{-}.

The BCP elements can also be calculated with other combinations of the eight IMF sector potential distributions. Some results of such calculations are presented in Fig. 3. Each panel shows the relationship and IMF sectors used for the calculation of each of the BCP elements. The potential values of the foci are indicated below each panel, and the total potential difference is presented on the upper right-hand side. For the calculation of the BCP elements, we used the following relationships:

$$\begin{aligned} U_z^{-} &= (\mathrm{Sector\ 3} + \mathrm{Sector\ 5} - 2U_0)/6.17 \\ U_z^{+} &= (\mathrm{Sector\ 1} + \mathrm{Sector\ 7} - 2U_0)/5.66 \\ U_y^{+} &= (\mathrm{Sector\ 3} - \mathrm{Sector\ 5})/7.10 \\ U_y^{+} &= (\mathrm{Sector\ 1} - \mathrm{Sector\ 7})/6.94. \end{aligned} \quad (5)$$

Figures 2 and 3 present BCP elements, which are controlled by the IMF *By* and *Bz* components obtained independently from different original data. They are practically identical with respect to the following: the number and orientation of convection cells; position of their foci; potential difference between foci, which only differ by 0.7 kV for U_z^{-}, by

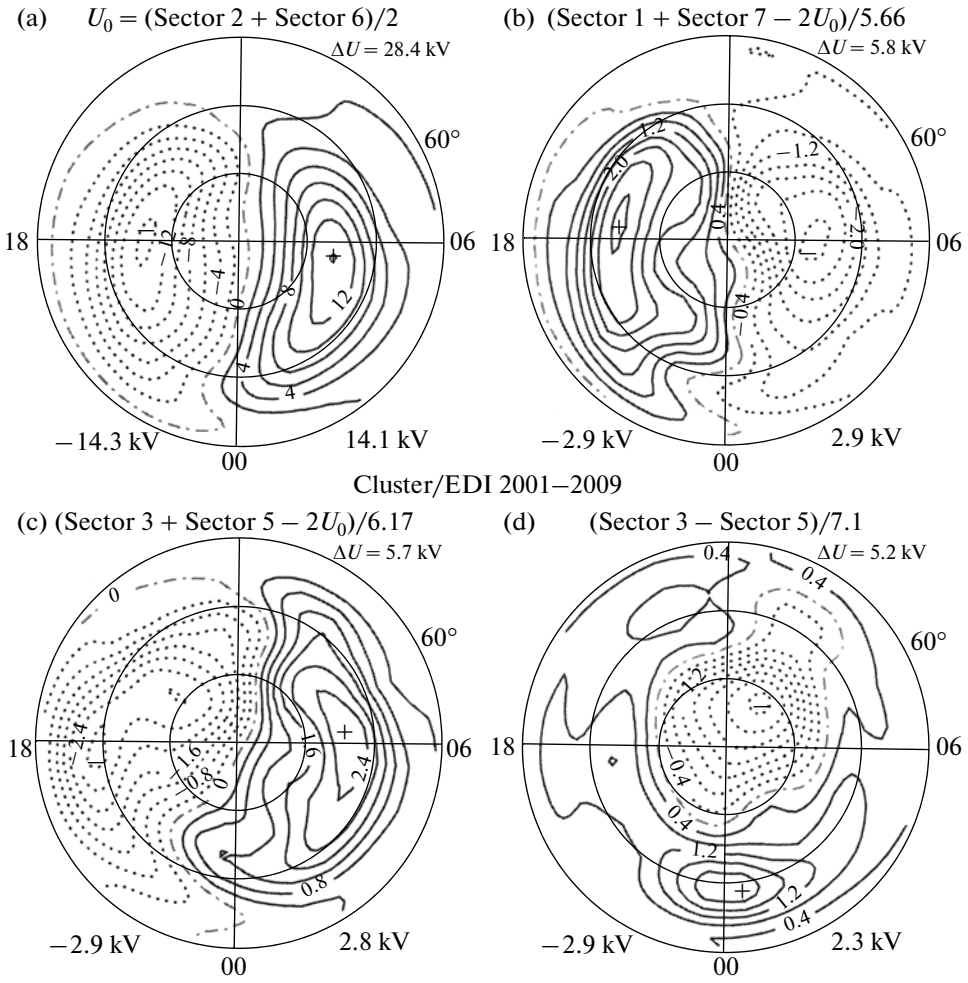

Fig. 2. BCP elements, derived from Cluster EDI observations for various IMF orientations, as presented in Fig. 1. Their entirety constitutes an ionospheric convection model depending on the IMF: (a) the potential distribution part, which is independent of IMF *Bz* and *By*; (b) isolines of the potential contribution for positive *Bz* values, normalized to *Bz* = +1 nT; (c) the same for negative *Bz* values (i.e., *Bz* = −1 nT); (d) potential distribution for the normalized *By* = 1 nT. The relationships for the calculation of the respective elements are presented above each panel.

0.5 kV for U_z^+, and by 0.3 kV for cells U_y^+ within the polar cap. This good agreement between BCP elements lends credence to their validity, because they result in approximately the same pattern, although they were derived from different (independent) plasma drift measurements of the EDI.

The spatiotemporal convection pattern and cross-polar cap potential drop ΔU at high latitudes were obtained from EDI data for different IMF orientations within sectors of the $\alpha = 45°$ conus angle width. A compelling question is therefore whether the convection pattern changes for smaller conus angles α. Förster et al. (2008) considered pattern changes (for a near-northward IMF) at a 5° IMF orientation while keeping constant the 45° cone width. Here, we estimated the influence of varying α on the characteristics and intensity of high-latitude convection when analysing EDI data for both hemispheres between February 2001 and April 2009. We used the eighth-order harmonics for our analysis and diminished $\alpha = 45°$ in steps of 10°. The convection characteristics were practically kept constant down to $\alpha = 10°$; i.e., a two-cell plasma convection pattern of the main cells in the morning and evening sides persisted for all sectors and an additional pair of high-latitude dayside cells appeared for the northward IMF (Sector 0). The data coverage downgraded continuously with diminishing angle α, in particular for magnetic latitudes < 75°, and changed for the worst when $\alpha = 7.5°$, where even the characteristics of the derived potential pattern changed. When decreasing α from 45° to 10°, the ΔU cross-polar cap potential difference stayed near 20 ± 2 kV for the northward-oriented Sectors 1 and 7 and at a lower level of 13 ± 2 kV for Sector 0. For the east–west orientation of the IMF, ΔU remianed within 35 ± 3 kV for Sectors 2 and 6, while it was 52 ± 5 kV for the southward IMF sectors 3 and 5 and 55 ± 6 kV for Sector 4. There-

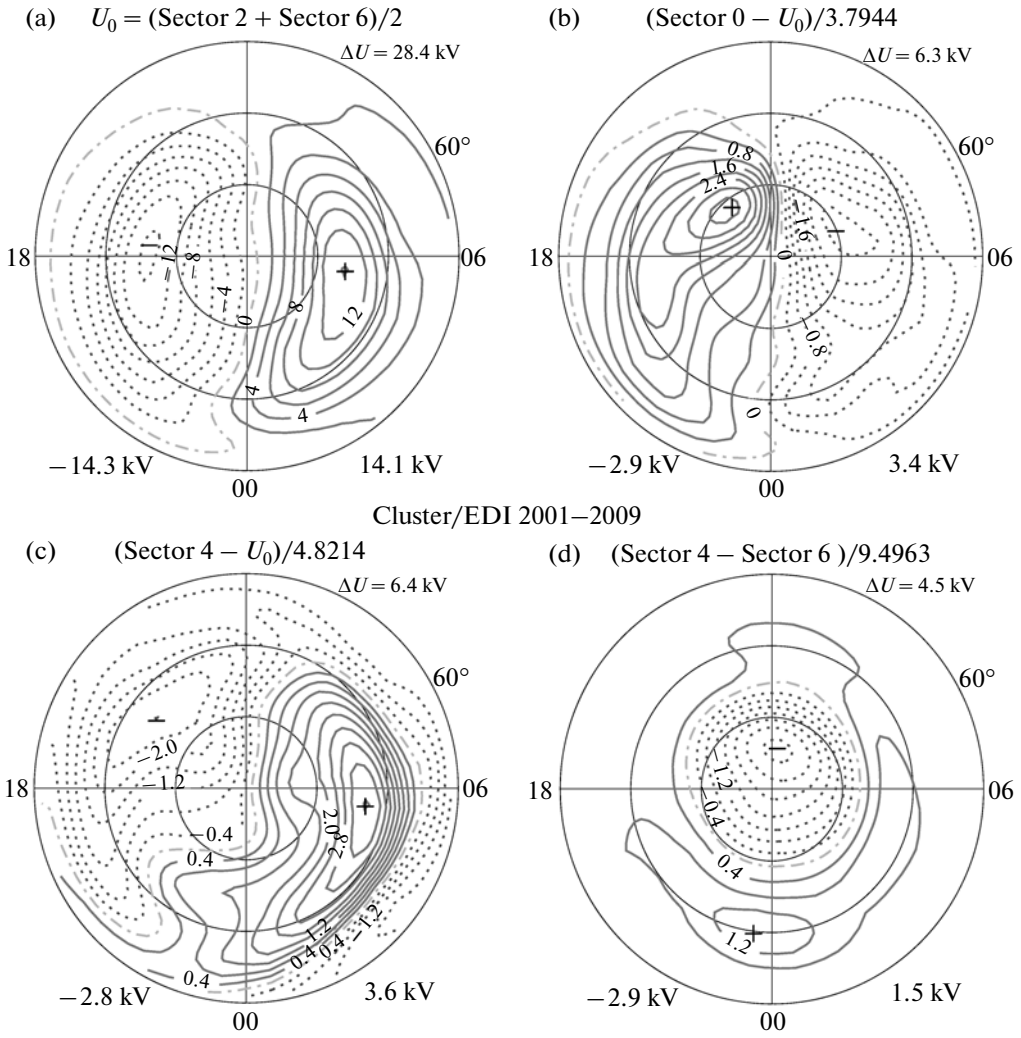

Fig. 3. Same as in Fig. 2 but using relationships (4) for the calculation of the BCPs instead of those shown in Fig. 2.

fore, a reduction in cone angle α from 45° to 10° does not lead to any significant change in convection characteristics nor changes its intensity by more than 10%.

5. IMF *Bx* COMPONENT AND PLASMA CONVECTION IN THE HIGH-LATITUDE IONOSPHERE

Literature contains different, even completely contrary, opinions regarding the influence of the IMF *Bx* component on geophysical processes at high latitudes. Yahnin and Sergeev (1981), Crooker (1986), Cowley et al. (1991), Belenkaya (1998), Blomberg et al. (2005), Alexeev et al. (2007), Newell et al. (2009), and Peng et al. (2010) advance the view that *Bx* has a considerable influence, while the studies of Levitin et al. (1982) and Newell et al. (1989) did not succeed to find any significant influence of this IMF component on high-latitude current systems. The difficulty to assign any IMF *Bx* dependence is due to the essential sector structure of the IMF in the ecliptic plane, which consists of two different sectors, in each of which the *Bx* and *By* components of the IMF vector have opposite signs. Analysing geomagnetic variations in the near-polar region, Friis-Christensen et al. (1972) and Sumaruk and Feldstein (1973) concluded that the sector structure effect is dominated by the *By* component. This conclusion was based on event studies of geomagnetic variations in the polar cap and their correlation with IMF vector components during intervals when the sector structure was unsettled and these two vector components had the same sign. Their results are nowadays generally accepted and all published high-latitude statistical convection models include only the dependence on the IMF *By* and *Bz* components to describe the spatiotemporal convection pattern.

The large amount of EDI drift measurements at high latitudes with the help of the Cluster/EDI satellites during more than 8.5 years allows us to reinvesti-

Table 3. Cross-polar cap potential difference ΔU between the main (nighttime) convection foci in kilovolts for Cluster/EDI data for 2001–2009, sorted separately for an IMF directed toward the Sun ($Bx > 0$) and away from the Sun ($Bx < 0$)

IMF Sector	ΔU, kV, Northern Hemisphere		ΔU, kV, Southern Hemisphere	
	$Bx > 0$	$Bx < 0$	$Bx > 0$	$Bx < 0$
0	15.5	15.4	11.5	11.8
1	21.8	24.6	22.9	23.4
2	35.4	34.0	37.9	37.9
3	50.8	44.5	47.2	48.2
4	58.5	54.6	52.5	57.4
5	44.2	59.4	49.5	49.7
6	32.9	35.9	33.4	34.8
7	17.7	24.2	21.9	20.6

Table 4. Cross-polar cap potential drop ΔU between the convection foci for BCP U_0 and U_y^+ based on Cluster/EDI data for 2001–2009

BCP element	Northern Hemisphere		Southern Hemisphere	
	Method I	Method II	Method I	Method II
U_0	30.4	29.5	33.3	30.9
U_y^+	−2.9	−3.0	2.8	2.5

gate the influence of the IMF *Bx* component on the ionospheric plasma convection. For this purpose, we divided the data into two subsets of about the same size with $Bx > 0$ (the IMF vector is directed toward the Sun), on the one hand, and $Bx < 0$ (the IMF is directed away from the Sun), on the other hand. Each subset was then sorted for the same eight sectors of IMF orientation in the GSM *YZ* plane as before and the electric potential distributions in the ionosphere at an altitude of 400 km were calculated based on the same method as described in Sections 2 and 3. The characteristics of the potential distribution in all eight sectors resemble the convection pattern shown in Fig. 1, which confirms that even half of the data is sufficient to get stable potential distributions. The mean IMF *Bx* amplitude varies in different sectors from about 2 to 4 nT; smaller values of ~2 nT are met in sectors, where *Bx* and *By* have the same sign, while values of ~4 nT are in sectors with opposite signs.

Table 3 shows the cross-polar cap potential difference between the morning and evening side foci of all eight sectors for both Northern and Southern hemisphere (separately for $Bx > 0$ and $By < 0$ conditions). One may conclude from these data that not only the general characteristics of the convection pattern are retained, but also the regularity of the cross-polar cap potential difference changes: ΔU increases monotonically from Sector 0 to Sector 4 and reduces again for negative *By* values from Sector 4 to Sector 0. In the Southern Hemisphere, this regularity is valid everywhere, while in the Northern Hemisphere there is one exception for Sector 5 when $Bx < 0$. We suppose that this exception may be explained by an insufficient number of data points, firstly, because of the orbital characteristics of the Cluster satellites with their apogee turning southward, which favors the data on the Southern Hemisphere, and, secondly, because of the generally smaller number of data points with similar *Bx* and *By* signs. The compilation of ΔU values of both hemispheres with opposite *Bx* orientations (Table 3) does not give significant evidence for a *Bx* dependence of the cross-polar potential drop.

We further made an attempt to find parts of the high-latitude convection which might be controlled by IMF *Bx*. As described below, this attempt considered two different methods which are based on different assumptions.

The first method draws upon the assumption that the IMF *Bx* component does not have an effect on convection in the case of equally directed *Bx* and *By*, i.e., in the Northern Hemisphere for $Bx > 0$ this is Sectors 1–3, while for $Bx < 0$ this is valid for Sectors 5–7. In further calculations, we only consider Sectors 2 and 6, where the influence of IMF *Bz* practically disappears and the convection pattern therefore becomes simpler.

The second method draws upon the circumstance that the Earth's dipole magnetic field lines over the northern polar cap region have an opposite direction to IMF field lines for $Bx < 0$, but over the southern polar cap region this happens for $Bx > 0$. An opposite direction of the IMF and the magnetospheric tail magnetic field constitutes a favorable condition for the penetration of solar wind plasma into the polar cap region (Newell et al., 2009). An enhanced flow of soft energetic particles can likewise affect convection due to an increased level of ionization of the upper atmosphere.

More details regarding the methodology of various trials to deduce *Bx*-dependent parts of convection from Cluster/EDI data and the results obtained are described in (Förster et al., 2011).

Using the above relationships, we get a convection pattern for IMF-independent element U_0, as well as elements, which are controlled by the IMF $\pm By$ and $\pm Bx$ components ($U_y^{\pm}$ and $U_x^{\pm}$, respectively). In all cases, the U_0 element describes two-cell convection with foci on the morning and evening sides and antisolar convection across the polar cap, while the $\pm By$ element specifies one-cell convection within the polar cap, the focus of which is situated close to the geomagnetic pole with circulation in the Northern (Southern) Hemisphere in a counter-clockwise (CCW) (clockwise

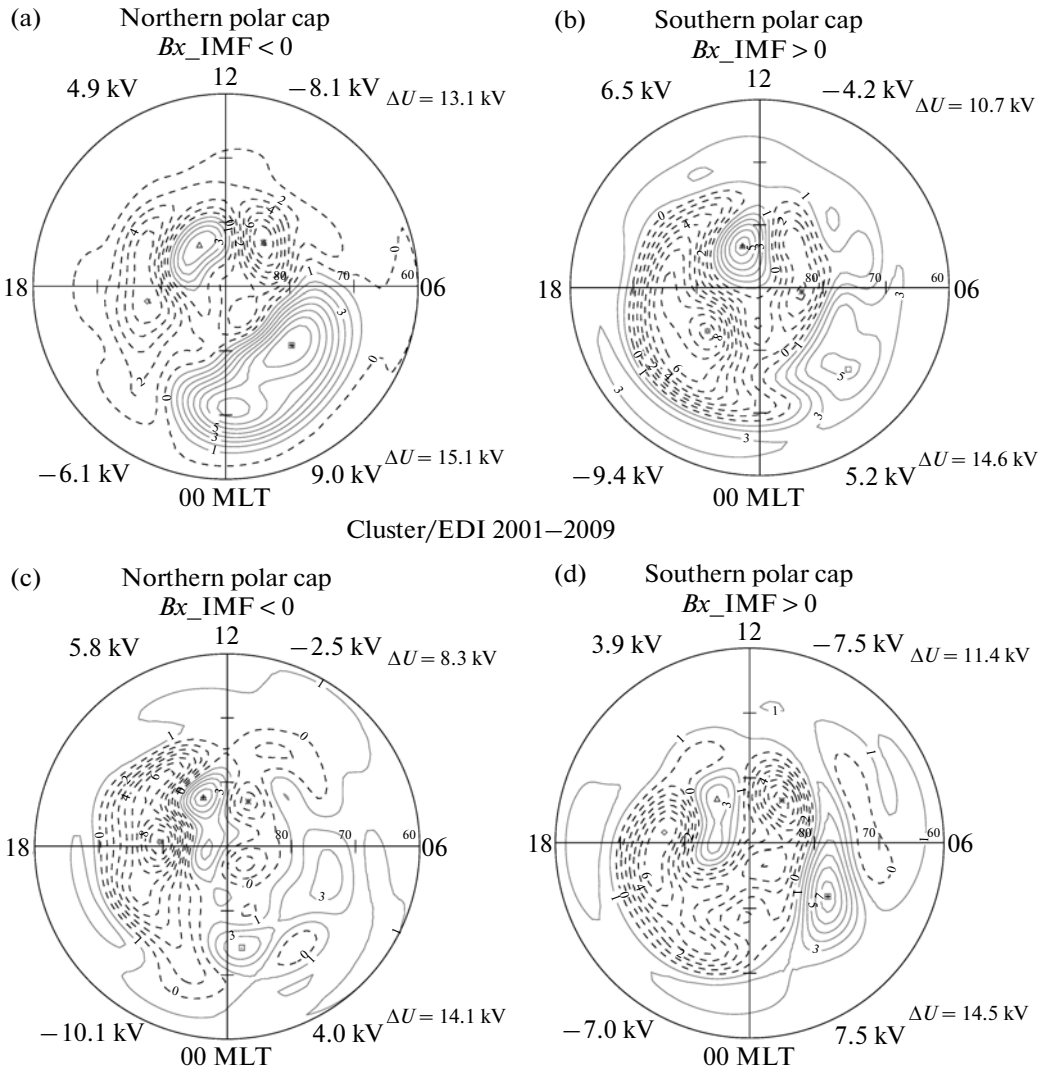

Fig. 4. High-latitude convection pattern of Sector 0 obtained from Cluster C1–C3 EDI observations during the interval February 2001–September 2009. The numbers indicate the potential peak values of the corresponding foci (as for Sector 0 in Fig. 1). (a) northern polar cap with IMF $Bx < 0$, (b) northern polar cap with $Bx > 0$, (c) southern polar cap with $Bx < 0$, and (d) Southern polar cap with $Bx > 0$.

(CW)) direction for $By > 0$ and CW (CCW) for $By < 0$. Cross-polar cap potential drop ΔU for U_0 and the potential values of the U_y^+ elements are given in Table 4.

The characteristics of the potential pattern and the ΔU values of BCP elements U_0 and $U_y^\pm$ (Table 4) show good agreement for both methods, as well as with the previously determined values in Fig. 2 with $\Delta U_0 = 28.4$ kV and $\Delta U_y^+ = -2.9$ kV. Such a good correspondence can serve as an additional valid argument in favor of the legitimacy of the assumption adopted for the calculation of the BCPs.

The IMF *Bx* dependence of characteristics and the intensity of the convection pattern for the main (nighttime) cells for all IMF orientations and in Sectors 2 and 6 (for $\pm By$) is not so clear. There is no regular systematic convection pattern, but rather some small randomly distributed vortices. The isolines are very irregular and the vortices have peaks, which are several times smaller than those related to the IMF *By* and *Bz* components. No specific distributions were observed which could be related to the sign of IMF *Bx* or to hemispheric differences. We could not therefore reveal any conclusive evidence for the presence of an IMF *Bx* dependence in the convection pattern, its characteristics, or intensity for the given situation.

On the other hand, the conducted analysis of potential drops between high-latitude dayside cells, as they appear for IMF $Bz > 0$, provides some reason to assume a slight IMF *Bx* dependence.

Figure 4 shows the potential pattern in Sector 0 for the Northern and Southern hemispheres for opposite

orientations of IMF *Bx*. There appear 4-cell convection patterns during all of these situations with a pair of sunward-directed cells on the dayside with foci before and after midday at geomagnetic latitudes between 82° and 84°. The potential drop between dayside high-latitude foci shows some correlation with the IMF *Bx* component. It is larger for antiparallel orientations of geomagnetic field lines in the magnetospheric tail and the IMF *Bx* component. For the northern polar cap, this corresponds to an IMF orientation with $Bx < 0$; for the southern polar cap, to $Bx > 0$.

6. CONCLUSIONS

Based on complementary analyses of the present study we conclude the following:

1. The BCP elements of the basic convection pattern (BCP), which were derived by different methods and by using independent data, are qualitatively identical in the shape and orientation of convection cells, as well as in the position of their focal points. The cross-polar potential difference in the Northern Hemisphere for the IMF-independent part amounts to $\Delta U(U_0) = 29.4 \pm 0.7$ kV, while the IMF-dependent components of the BCPs are $\Delta U(U_y^+) = -2.8 \pm 0.2$ kV for $By < 0$, $\Delta U(U_z^-) = 6.0 \pm 0.3$ kV for $Bz < 0$, and $\Delta U(U_z^+) = 6.0 \pm 0.2$ kV for $Bz > 0$. The agreement of the BCP elements within a few percentage points lends credence to the correctness of their quantitative estimation, because they were obtained from independent plasma drift measurements with the EDI.

2. The methodology and the results of the spatiotemporal potential distribution, which was obtained by Förster et al. (2009), are also affirmed with respect to (a) the upgrading of the spherical harmonics from the eighth to the tenth order during modelling and (b) the reduction in the sector's IMF conus angle width from 45° to 10°.

3. There is no significant evidence for an IMF *Bx* dependence of the convection pattern for the main (nighttime) cells. The potential difference between pairs of dayside high-latitude convection cells of Sector 0 (IMF $Bz > 0$) appears to be larger for an antiparallel orientation of the magnetic field of the magnetospheric tail and in the solar wind (dependence on IMF *Bx*).

ACKNOWLEDGMENT

The work at the GFZ German Research Center for Geosciences, Potsdam (M. Förster), was supported by Deutsche Forschungsgemeinschaft (DFG), the research at the University of Bergen (S.E. Haaland) was supported by the Norwegian Research Council, and the work at IZMIRAN (L.I. Gromova, L.A. Dremukhina, and A.E. Levitin) was supported by the Russian Foundation for Basic Research (grant no. 11-0500306). We thank the ACE SWEPAM and MAG instrument teams and the ACE Science Center for providing ACE data.

REFERENCES

Alexeev, I.I., Belenkaya, E.S., Bobrovnikov, S.Yu., Kalegaev, V.V., Cummnok, J.A., and Blomberg, L.G., Magnetopause Mapping to the Ionosphere for Northward IMF, *Ann.Geophys.*, 2007, vol. 25, no. 12, pp. 2615–2625.

Baker, J.B.H., Greenwald, R.A., Ruohoniemi, J.M., Förster, M., Paschmann, G., Donovan, E.F., Tsyganenko, N.A., Quinn, J.M., and Balogh, A., Conjugate Comparison of Super Dual Auroral Radar Network and Cluster Electron Drift Instrument Measurements of $E \times B$ Plasma Drift, *J. Geophys. Res.*, 2004, vol. 109A, pp. 01209–01229; doi:10.1029/2003JA009912.

Balogh, A., Carr, C.M., Acuna, M.H., et al., The Cluster Magnetic Field Investigation: Overview of In-Flight Performance and Initial Results, *Ann.Geophys.,* 2001, vol. 19, no. 10, pp. 1207–1217.

Belenkaya, E.S., High-Latitude Ionospheric Convection Patterns Dependent on the Variable IMF Orientation, *J. Atmos. Sol.–Terr. Phys.*, 1998, vol. 60, no. 13, pp. 1343–1354.

Blomberg, L.G., Cummnok, J.A., Alexeev, I.I., Belenkaya, E.S., Bobrovnikov, S.Yu., and Kalegaev, V.V., Transpolar Aurora: Time Evolution, Associated Convection Patterns, and a Possible Cause, *Ann. Geophys.,* 2005, vol. 23, no. 5, pp. 1917–1930.

Cowley, S.W.H., Morelli, J.P., and Lockwood, M., Dependence of Convective Flow and Particle Precipitation in the High-Latitude Dayside Ionosphere on the *X* and *Y* Components of the IMF, *J. Geophys. Res.*, 1991, vol. 96A, pp. 5557–5564.

Crooker, N.U., An Evolution of Antiparallel Merging, *Geophys. Res. Lett.,* 1986, vol. 13, no. 10, pp. 1063–1066.

Eriksson, A.I., Andre, M., Klecker, B., et al., Electric Field Measurements on CLUSTER: Comparing the Double-Probe and Electron Drift Techniques, *Ann. Geophys.,* 2006, vol. 24, no. 1, pp. 275–289.

Feldstein, Y.I. and Levitin, A.E., Solar Wind Control of Electric Fields and Currents in the Ionosphere, *J. Geomagn. Geoelectr.*, 1986, vol. 38, pp. 1143–1182.

Förster, M., Paschmann, G., Haaland, S.E., et al., High-Latitude Plasma Convection from Cluster EDI: Variances and Solar Wind Correlations, *Ann. Geophys.,* 2007, vol. 25, no. 7, pp. 1691–1707.

Förster, M., Haaland, S.E., Paschmann, G., et al., High-Latitude Plasma Convection during Northward IMF as Derived from In-Situ Magnetospheric Cluster EDI Measurements, *Ann. Geophys.,* 2008, vol. 26, no. 9, pp. 2685–2700.

Förster, M., Feldstein, Y.I., Haaland, S.E., Dremukhina, L.A., Gromova, L.I., and Levitin, A.E., Magnetospheric Convection from Cluster EDI Measurements Compared with the Ground-Based Ionospheric Convection Model IZMEM, *Ann. Geophys.,* 2009, vol. 27, no. 8, pp. 3077–3087.

Förster, M., Feldstein, Y.I., Gromova, L.I., Dremukhina, L.A., Levitin, A.E., and Haaland, S.E., Plasma Convection in the High-Latitude Ionosphere Deduced from Clus-

ter EDI Data and IMF *Bx* Component, *Proc. 34th Apatity Annual Seminar "Physics of Auroral Phenomena"*, Apatity, 2011, pp. 42–45.

Friis-Christensen, E., Lassen, K., Wilhjelm, J., Wilcox, J.M., Gonsalez, W., and Colburn, D.S., Critical Component of the Interplanetary Magnetic Field Responsible for Large Geomagnetic Effects in the Polar Cap, *J. Geophys. Res.*, 1972, vol. 77, no. 19, pp. 3371–3376.

Haaland, S.E., Paschmann, G., Förster, M., et al., High-Latitude Plasma Convection from Cluster EDI Measurements: Method and IMF-Dependence, *Ann. Geophys.,* 2007, vol. 25, no. 1, pp. 239–253.

Haines, G.V., Spherical Cap Harmonic Analysis, *J. Geophys. Res.*, 1985, vol. 90B, pp. 2583–2591.

Kabin, K., Rankin, R., Marchand, R., et al., Dynamic Response of Earth's Magnetosphere to *By* Reversals, *J. Geophys. Res.,* 2003, vol. 108A, pp. 1132–1143; doi:10.1029/ 2002JA009480.

Levitin, A.E., Afonina, R.G., Belov, B.A., and Feldstein, Y.I., Geomagnetic Variations and Field-Aligned Currents at Northern High-Latitudes and Their Relations to Solar Wind Parameters, *Philos Trans. R. Soc. (London), Ser. A*, 1982, vol. A304, pp. 253–301.

Newell, P.T., Meng, C.-I., Sibeck, D.G., and Lepping, R., Some Low-Altitude Cusp Dependencies on the Interplanetary Magnetic Field, *J. Geophys. Res.*, 1989, vol. 94A, pp. 8921–8927.

Newell, P.T., Liou, K., and Wilson, G.R., Polar Cap Particle Precipitation and Aurora: Review and Commentary, *J. Atmos. Sol.–Terr. Phys.*, 2009, vol. 71, no. 2, pp. 199–215.

Papitashvilli, V.O. and Rich, F.J., High Latitude Ionospheric Convection Models Derived from DMSP Ion Drift Observations and Parametrized by the Interplanetary Magnetic Field Strings and Direction, *J. Geophys. Res.,* 2002, vol. 107A, pp. 1198–1210; doi:10.1029/ 2001JA000264.

Paschmann, G., Quinn, J.M., Torbert, R.B., et al., The Electron Drift Instrument on Cluster: Overview of First Results, *Ann.Geophys.,* 2001, vol. 19, no. 10, pp. 1273–1288.

Peng, Z., Wang, C., and Hu, Y.Q., Role of IMF *Bx* in the Solar Wind–Magnetosphere–Ionosphere Coupling, *J. Geophys. Res.*, 2010, vol. 115A, pp. 8224–8230; doi:10.1029/2010A015454.

Sumaruk, P.V. and Feldstein, Y.I., Sector Structure of IMF and Magnetic Disturbances in the Polar Region, *Kosm. Issled.,* 1973, vol. 11, no. 1, pp. 155–160.

Weimer, D.R., Ober, D.M., Maynard, N.C., Collier, M.R., McComas, D.J., Ness, N.F., Smith, C.W., and Watermann, J., Predicting Interplanetary Magnetic Field (IMF) Propagation Delay Times Using the Minimum Variance Technique, *J. Geophys. Res.*, 2003, vol. 108A, pp. 1026–1037; doi:10.1029/2002JA009405.

Yahnin, A.G. and Sergeev, V.A., Polar Cap Auroras Depending on the IMF Orientation and Substorms: Certain Morphological Features, *Polyarn. Siyaniya Svechenie Nochnogo Neba*, 1981, no. 28, pp. 27–34.